Computers & Geosciences 106 (2017) 181–189

Contents lists available at ScienceDirect

Computers & Geosciences

journal homepage: www.elsevier.com/locate/cageo

Research paper

Wind wave analysis in depth limited water using OCEANLYZ, A MATLAB toolbox☆

Arash Karimpour[a,*], Qin Chen[b,c]

[a] Louisiana Sea Grant Louisiana State University, Baton Rouge, LA 70803, USA
[b] Department of Civil and Environmental Engineering, Louisiana State University, Baton Rouge, LA 70803, USA
[c] Center for Computation and Technology, Louisiana State University, Baton Rouge, LA 70803, USA

ARTICLE INFO

Keywords:
Measured wind wave analysis
Frequency and time domains wave data analysis
OCEANLYZ
MATLAB toolbox

ABSTRACT

There are a number of well established methods in the literature describing how to assess and analyze measured wind wave data. However, obtaining reliable results from these methods requires adequate knowledge on their behavior, strengths and weaknesses. A proper implementation of these methods requires a series of procedures including a pretreatment of the raw measurements, and adjustment and refinement of the processed data to provide quality assurance of the outcomes, otherwise it can lead to untrustworthy results.

This paper discusses potential issues in these procedures, explains what parameters are influential for the outcomes and suggests practical solutions to avoid and minimize the errors in the wave results. The procedure of converting the water pressure data into the water surface elevation data, treating the high frequency data with a low signal-to-noise ratio, partitioning swell energy from wind sea, and estimating the peak wave frequency from the weighted integral of the wave power spectrum are described. Conversion and recovery of the data acquired by a pressure transducer, particularly in depth-limited water like estuaries and lakes, are explained in detail.

To provide researchers with tools for a reliable estimation of wind wave parameters, the Ocean Wave Analyzing toolbox, OCEANLYZ, is introduced. The toolbox contains a number of MATLAB functions for estimation of the wave properties in time and frequency domains. The toolbox has been developed and examined during a number of the field study projects in Louisiana's estuaries.

1. Introduction

Wind wave measurements and analysis in depth-limited water bodies, like estuaries and lakes, are of general interest for coastal researchers. There are a number of methods in the literature to assess the measured wave data and estimate the wave parameters. In depth-limited environments, additional steps are needed to properly implement these methods and to acquire reliable results. This requires the knowledge on how each of these methods behaves and how they influence the outcomes.

Pressure transducers are common instruments used for wave measurements in a depth-limited environment. Low cost, simple operation, acceptable accuracy and being submersible promote their popularity (e.g. Cavaleri, 1980; Jones and Monismith, 2007). Being submersible provides convenient deployment and enhanced protection, particularly in areas with considerable marine traffic. However, it can cause alteration in wave data as the underwater recorded data are affected by phenomena such as the presence of currents resulting in a Doppler-shift effect, and wave energy attenuation in water depth causing information loss (e.g. Cavaleri, 1980). A combination of the shallow environment and under water measurements adds potential issues to the data analysis, requiring additional steps such as converting the water pressure data into the water surface elevation data, treating the high frequency data with a low signal-to-noise ratio, and partitioning swell energy from wind sea to get proper outcomes (e.g. Cavaleri, 1980; Tsai et al., 2001; Smith, 2002).

The adequacy of the linear wave theory to analyze pressure transducer data in deep water has been well established in the literature. Although, higher order non-linear terms (e.g., Lee and Wang, 1984; Hashimoto et al., 1997) and experimental relationships (e.g. Wang et al., 1986; Kuo and Chiu, 1994) were proposed to improve the quality of wave properties calculated from pressure transducer data, it has been shown that for many practical applications, the linear wave theory is sufficiently accurate for analyzing data measured by a

☆ http://download.cnet.com/Oceanlyz/3000-2054_4-75833686.html.

* Corresponding author.
E-mail address: akarimp@g.clemson.edu (A. Karimpour).

http://dx.doi.org/10.1016/j.cageo.2017.06.010
Received 2 May 2016; Received in revised form 20 December 2016; Accepted 7 June 2017
Available online 16 June 2017
0098-3004/

Nomenclature

a_n	amplitudes (Fourier series coefficient)
b_n	amplitudes (Fourier series coefficient)
c_n	amplitudes (Fourier series coefficient)
C	wave celerity
d_s	pressure measurement distance (pressure sensor location) from the bed
D	time series duration
E_w	wave energy
f	frequency
f_{cmax}	high-cutoff frequency (low-pass filter)
f_{cmin}	low-cutoff frequency (high-pass filter)
f_l	lower limit of spectrum for sea wave and swell partitioning
f_m	mean wave frequency
$f_{maxpcorr}$	high-cutoff frequency associated with K_{pmin}
$f_{maxpcorr-L}$	the $f_{maxpcorr}$ estimated by linear wave theory
f_{mPM}	mean wave frequency of the Pierson-Moskowitz spectrum
f_p	peak wave frequency
f_s	sampling frequency
f_{sep}	frequency that separates wind sea and swell wave energies
f_{tail}	high-cutoff frequency for replacing noise with an empirical spectrum tail
f_u	upper limit of spectrum for sea wave and swell partitioning
Δf	frequency interval
Δf_{tr}	frequency range for K_{pmin} transition before and after $f_{maxpcorr}$
g	gravitational acceleration
h	local water depth
h_s	sensor depth
H	wave height
H_{m0}	zero-moment wave height
H_{rms}	root mean square (*rms*) wave height
H_s	significant wave height
H_z	zero-crossing mean wave height
k	wave number
k_0	deep-water wave number
k_{max-L}	wave number associated with K_{pmin-L}
K_p	dynamic pressure to the surface elevation conversion factor (pressure response factor)
K_{pmin}	minimum value of K_p to prevent the over-estimation of the wave energy
K_{pmin-L}	the K_{pmin} estimated by linear wave theory
L	wave length
L_{min-L}	wave length associated with the smallest linear wave can be sensed by pressure sensor
L_p	wave length associated with f_p (peak wave length)
m_0	zero-moment of the wave energy spectrum
m_n	the n^{th} moment of the wave energy spectrum
N	total number of waves in the dataset
N_{Cor}	correction factor
P	static pressure
P_0	total pressure
q	dynamic pressure
$RMSE$	root-mean-square error
S_{PP}	dynamic pressure power spectral density
$S_{\eta\eta}$	water surface elevation power spectral density
t	time
t_{br}	burst duration
Δt_{bl}	interval between measured blocks of data
Δt_s	time interval between two sequential data points
T	wave period
T_{m01}	mean wave period
T_{m02}	mean zero-crossing period
T_p	peak wave period
T_s	significant wave period
T_z	zero-crossing mean wave period
U_{10}	wind velocity at 10 m above the surface
X	expected value
Y	estimated value
z	upward vertical axis with zero at water surface
η	water surface elevation
$\eta(t)$	Fourier series of the water surface elevation
η_{rms}	root mean square (*rms*) of the surface elevation
ρ	water density
σ_η	standard deviation of the surface elevation
$\varnothing_n$	phase
Φ	transformation function from JONSWAP spectrum into TMA spectrum
ω	wave angular frequency

pressure transducer (e.g. Bishop and Donelan, 1987; Van Rijn et al., 2000; Tsai et al., 2001; Tsai, et al., 2005; Jones and Monismith, 2007). Still, as the wave travels to depth-limited water, like estuaries and lakes, implementing the linear wave theory requires additional steps to acquire accurate results.

The main goal of this paper is to present and discuss the steps that are required to attain a reliable estimation of wave parameters, particularly in shallow and intermediate water depth. A brief theoretical background is presented to describe the common methods for wave analysis, followed by explanation of their behaviors and the effect of influential parameters on their outcomes. Then, the sensitivity of each method is discussed and the reliability of the estimated wave parameters is explained. Next, the Ocean Wave Analyzing toolbox, OCEANLYZ, is presented. This toolbox contains a number of MATLAB functions for wave properties estimation in the time or frequency domain. It has been developed and used to analyze a number of field data sets measured in the depth-limited estuaries of Louisiana. As a result, the OCEANLYZ has evolved over time to address the data analysis issues encountered in these shallow environments. These types of toolboxes are developed in the literature to provide analysis tools for researchers (e.g., Landry et al., 2012). With a similar goal, OCEANLYZ provides researchers a reliable tool for estimation of the wave parameters, particularly in shallow and intermediate water.

2. Theoretical background

Commonly, wave data are recorded as a time series of data points with an equal spacing in time. Data sampling is briefly explained in Supplementary material A. The wave parameters can be calculated directly from the recorded data in the time domain, or the temporal signal can be transformed and assessed in the frequency domain.

2.1. Time domain analysis (zero-crossing method)

Wave properties can be calculated in the time domain using the zero-crossing method to analyze the data. In the zero-crossing method, data should initially be de-trended by removing the mean value of each burst from the data points captured within that burst. Note that if there is a moving average trend within the burst, then the data in that burst are not stationary (see Supplementary material A). After the data are de-trended, each wave can be defined by two successive points where data cross up the horizontal axis (upward zero-crossing) or cross down

the horizontal axis (downward zero-crossing). Next, assuming the wave heights follow the Rayleigh distribution, the wave properties can be defined as (e.g. Dean and Dalrymple, 1991; Holthuijsen, 2007; McCormick, 2009):

$$H_z = \frac{1}{N}\sum_{i=1}^{N} H_i \tag{1-a}$$

$$H_{rms} = \left(\frac{1}{N}\sum_{i=1}^{N} H_i^2\right)^{0.5} = 2\sqrt{2}\eta_{rms} = \frac{2}{\sqrt{\pi}}H_z \approx 1.13H_z \tag{1-b}$$

$$H_s = \frac{1}{N/3}\sum_{i=1}^{N/3} H_i \approx \sqrt{2}H_{rms} \tag{1-c}$$

$$T_z = \frac{1}{N}\sum_{i=1}^{N} T_i \tag{1-d}$$

$$T_s = \frac{1}{N/3}\sum_{i=1}^{N/3} T_i \tag{1-e}$$

where, N is a total number of the waves in the dataset, H and T are wave height and wave period, respectively, both sorted in a descending order, H_z is a zero-crossing mean wave height, H_{rms} is a root mean square (rms) wave height, η_{rms} is a root mean square of the water surface elevation, H_s is a significant wave height, T_z is a zero-crossing mean wave period, and T_s is a significant wave period.

2.2. Frequency domain analysis (spectral analysis method)

Another method to assess the data is to transform and analyze the dataset in the frequency domain. In this method, the measured data are transformed from the time domain to the frequency domain by using the Fast Fourier Transform (FFT) algorithm. Then, a wave energy spectrum is calculated as (e.g. Chakrabarti, 1987; Holthuijsen, 2007; Reeve et al., 2012):

$$\eta(t) = \sum_{n=1}^{N}\left(a_n\cos(2\pi f_n t) + b_n\sin(2\pi f_n t)\right) \tag{2-a}$$

$$\eta(t) = \sum_{n=1}^{N} c_n\cos(2\pi f_n t + \varnothing_n) \tag{2-b}$$

$$S_{\eta\eta}(f_n) = \frac{1}{\Delta f}\times\sum_{f_n}^{f_n+\Delta f}\left(\frac{1}{2}c_n^2\right) = \lim_{\Delta f\to 0}\frac{1}{\Delta f}\left(\frac{1}{2}c_n^2\right) \tag{2-c}$$

where, η is a surface elevation, t is time, $\eta(t)$ is the Fourier series of the surface elevation, a_n, b_n and c_n are amplitudes (i.e. Fourier series coefficients, where $c_n^2 = a_n^2+b_n^2$), $\varnothing_n$ is a phase (where $\tan\varnothing_n = -b_n/a_n$), $f_n = n/D$ is a frequency, $S_{\eta\eta}$ is a water surface elevation power spectral density, $\Delta f = 1/D$ is a frequency interval, and D is the time series duration. Then, the wave properties are defined as:

$$m_n = \int_0^{\infty} S_{\eta\eta}(f)f^n df \approx \sum_{i=1}^{N} S_{\eta\eta,i}\times f_i^n\times\Delta f_i \tag{3-a}$$

$$m_0 = \int_0^{\infty} S_{\eta\eta}(f)df = \sigma_\eta^2 \tag{3-b}$$

$$H_{m0} = 4\sigma_\eta = 4\sqrt{m_0} = 4\sqrt{\int_0^{\infty} S_{\eta\eta}(f)df} \approx 4\sqrt{\sum_{i=1}^{N} S_{\eta\eta,i}\times\Delta f_i} \tag{3-c}$$

$$T_p = \frac{1}{f_p} \tag{3-d}$$

$$T_{m01} = \frac{m_0}{m_1} \tag{3-e}$$

$$T_{m02} = \sqrt{\frac{m_0}{m_2}} \tag{3-f}$$

where m_n is the n^{th} moment of the wave energy spectrum, m_0 is a zero-moment of the wave energy spectrum, σ_η is a standard deviation of the water surface elevation, H_{m0} is a zero-moment wave height, T_p is a peak wave period, f_p is a peak wave frequency which is the frequency associated with the maximum value of the $S_{\eta\eta}$, T_{m01} is a mean wave period, and T_{m02} is a mean zero-crossing period. Relationships between the time and frequency domains are presented in Supplementary material B.

3. Data analysis and evaluation of effective factors on wave results

After the quality of the recorded data are evaluated and confirmed, additional steps are required to prepare the measured data for wave data analysis. In this section, the details of these steps and the effect of influential parameters within each step on the wave analysis outcomes are discussed.

3.1. Pressure data correction for dynamic pressure attenuation in depth

Pressure transducers are common instruments used for surface wave measurements. Recorded data from a pressure transducer contain two sets of signals. The first one is a hydrostatic pressure signal, which represents the sensor's depth and is used to define the water depth. The second one is a dynamic pressure signal, which is a result of the wave motion, i.e. water surface fluctuations, and is used to estimate wave properties. However, the dynamic pressure resulting from the water surface fluctuations begins to attenuate in the water column as a depth increases from the water surface towards the sea bed. As a result, dynamic pressure signals recorded by a pressure sensor are weaker compared to the original values at the water surface. The deeper the pressure sensor is located, the greater the pressure signal attenuates. Therefore, a dynamic pressure signal from a pressure transducer cannot be used directly for wave analysis, and requires the proper correction and preparation prior to analysis, otherwise it leads to an underestimation of the wave height and energy.

To account for the dynamic pressure loss at the sensor depth, at first the recorded pressure data are split into hydrostatic and dynamic pressures, and then, the dynamic pressure data are divided by a pressure response factor. The hydrostatic pressure is calculated by averaging the data over each burst. The dynamic pressure is acquired by de-trending the pressure signal, which is done by subtracting the hydrostatic pressure, i.e. the mean water depth, from the pressure signal. In other words, the mean pressure in each burst is the hydrostatic pressure, and the remaining values after the mean is subtracted from data in that burst are the dynamic pressures, given the fact that the data are stationary. Then, the original water surface elevation, which is accounting for dynamic pressure loss, is calculated as:

$$P_0(z=-h_s) = P + q = \rho g h_s + \rho g\eta K_p \tag{4-a}$$

$$h_s = \frac{P}{\rho g} \tag{4-b}$$

$$K_p(f, z=-h_s) = \frac{\cosh k(h+z)}{\cosh(kh)} = \frac{\cosh(kd_s)}{\cosh(kh)} \tag{4-c}$$

$$\eta = \frac{1}{K_p}\times\frac{q}{\rho g} \tag{4-d}$$

where P_0 is total pressure, P is static pressure and is equal to the mean water pressure, and q is dynamic pressure which represents the pressure due to water surface fluctuations. The z is an upward vertical axis with zero at the water surface. Considering a sensor depth to be equal to h_s, then the sensor location is $z=-h_s$. The ρ is water density, K_p is dynamic pressure to the surface elevation conversion factor, also called pressure response factor, h is local water depth, $f = 1/T$ is a wave frequency, and d_s is pressure measurement distance (pressure sensor location) from the bed. k is a wave number which is a function of the

wave frequency, f, and local water depth, h (e.g. Hunt, 1979; Beji, 2013, see Supplementary material C for details). η is the original water surface elevation, accounting for the dynamic pressure loss.

3.1.1. Pressure data correction in the time domain

In practice, an original water surface elevation can be obtained from the recorded data by using Eq. (4-d) in either the time or frequency domains. If pressure data are analyzed in the time domain, initially, the dynamic pressure data are converted to water surface elevation without applying K_p as $\eta_{ini} = q/\rho g$. By using the zero-crossing method, η_{ini} time series is split into a series of single waves. Next, given the fact that the wave period is not affected by pressure attenuation in the water column, wave period, wave number and K_p are calculated for each wave. Afterward, recorded data corresponding to each of the isolated waves are converted to the original water level, η, by using the associated K_p calculated for that wave in Eq. (4-d). Next, the entire time series of the original water level is reassembled by putting the corrected water level associated with each wave period together. Finally, the wave heights are obtained from corrected data by using the zero-crossing method.

3.1.2. Pressure data correction in the frequency domain

If the pressure data are analyzed in the frequency domain, initially, unreliable and noisy data associated with the low and high frequency ranges are removed from the dataset. For that purpose, a low-cutoff frequency, f_{cmin}, a so-called high-pass filter, and a high-cutoff frequency, f_{cmax}, a so-called low-pass filter, are implemented to remove the data with $f<f_{cmin}$ or $f>f_{cmax}$ from the dataset (Fig. 10). Then the water surface elevation power spectral density, $S_{\eta\eta}$, is estimated from the dynamic pressure power spectral density, S_{PP}, measured by the pressure sensor as:

$$S_{\eta\eta} = \frac{1}{K_p^2} \times S_{\eta_{lini}\eta_{lini}} = \frac{1}{K_p^2} \times \frac{S_{PP}}{\rho^2 g^2} \tag{5}$$

Then, the wave properties are obtained from $S_{\eta\eta}$ by using the spectral analysis method (e.g. Karimpour et al., 2016, 2017; Karimpour and Chen, 2016).

Some studies suggested that an implementation of the correction factor N_{Cor} in Eq. (4-d) as $\eta = (N_{Cor}/K_p) \times q/(\rho g)$ and in Eq. (5) as $S_{\eta\eta} = (N_{Cor}/K_p)^2 \times S_{PP}/(\rho^2 g^2)$ is required to account for a deviation of the measured wave profile from the linear wave theory (see Bishop and Donelan, 1987 for detail). Many studies have shown that an implementation of the linear wave theory, i.e. $N_{Cor}\approx 1$, is adequately accurate (within 5%) if the wave data are analyzed in the frequency domain (e.g. Bishop and Donelan, 1987; Kuo and Chiu, 1994; Townsend and Fenton, 1996; Tsai et al., 2005; Jones and Monismith, 2007).

3.1.3. Lower limit for K_p

Using the aforementioned method to account for pressure attenuation can lead to a potential error in wave data outcomes due to an unrealistic amplification of the short waves by K_p. Because of that, this method should be implemented with caution for shorter waves with large frequencies (small wave periods), in both the time and frequency domains. This is attributed to the fact that K_p is a function of the wave frequency (wave period) with a range of $0 \le K_p \le 1$, where $K_p = 1$ at $f = 0Hz$ (Fig. 1). As frequency increases, the K_p values start to decrease, resulting in small values for K_p in the higher frequencies. These small values can unrealistically magnify the associated water level fluctuation or wave energy obtained from Eqs. (4-d) and (5) (Figs. 2 and 10). To prevent that, a high-cutoff frequency, $f_{maxpcorr}$, should be selected to limit the minimum value of K_p to K_{pmin}, where $K_p = K_{pmin}$ for $f \ge f_{maxpcorr}$. This does not allow an amplification of the small waves in the time domain or an inflation of the high-frequency energies or even noises in the frequency domain. Therefore, it helps to prevent an over-estimation of the water surface oscillation or wave energy.

3.1.4. Theoretical approach to define lower limit for K_p

The values of $f_{maxpcorr}$ and the associated K_{pmin} depend on parameters such as a sensor depth, water depth and wave length. As it was noted above, the wave dynamic pressure attenuates in the water column from the water surface toward the bed. The free surface fluctuation effects, i.e. wave motion effects, nearly diminish in the water column as a depth becomes larger than half of the wave length, i.e. at $h \ge L/2$, where L is a wave length (Fig. 3). Therefore, if a pressure sensor depth is equal to h_s, then waves with $L/2 \le h_s$ cannot be detected by the sensor as their oscillation effects are almost damped before reaching the sensor depth. In other words, short waves with large wave frequencies (small wave periods) are less likely to be detected by a pressure transducer compared to long waves with small wave frequencies (large wave periods). This means that high frequency readings in a dataset, which are representing waves with $L/2 \le h_s$, are likely noise. Therefore, to avoid an amplification of the noise, the $f_{maxpcorr}$ or K_{pmin} should be selected to ensure that K_p is only being applied to waves whose effects reach the sensor's location.

The linear wave theory can be used to estimate the maximum wave frequency, $f_{maxpcorr}$, that K_p should be applied to. The linear wave theory indicates that the dynamic pressure from the wave oscillation decreases to near zero at a depth equal to half of the wavelength. Therefore, to estimate $f_{maxpcorr}$ and K_{pmin}, at first the wave length of the shortest linear wave, L_{min-L}, that can be detected by a pressure sensor at depth h_s is defined by $h_s = L_{min-L}/2$, where, the subscript L denotes that a value is estimated by the linear wave theory. It is equivalent to a wave with $k_{max-L} h_s = \pi$, where k_{max-L} is the maximum linear wave number associated with L_{min-L}. Considering sensor setup as described in Fig. 3, these can be re-written as $h_s = h - d_s = L_{min-L}/2$ and $k_{max-L}(h - d_s) = \pi$, which results in $k_{max-L} = \pi/(h - d_s)$. Then the minimum value for the pressure response factor estimated from the linear wave theory, K_{pmin-L}, is defined as:

$$K_{pmin-L}\,(f_{maxpcorr-L},\, z = -h_s) = \frac{\cosh(k_{max-L} d_s)}{\cosh(k_{max-L} h)} = \cosh\left(\frac{\pi}{h-d_s} d_s\right) / \cosh\left(\frac{\pi}{h-d_s} h\right) \tag{6}$$

then, the $f_{maxpcorr-L}$ which is a maximum frequency associated with K_{pmin-L} is:

$$\omega^2 = (2\pi f)^2 = gk \tanh(kh) \tag{7-a}$$

$$f = \frac{1}{2\pi}\sqrt{gk \tanh(kh)} \tag{7-b}$$

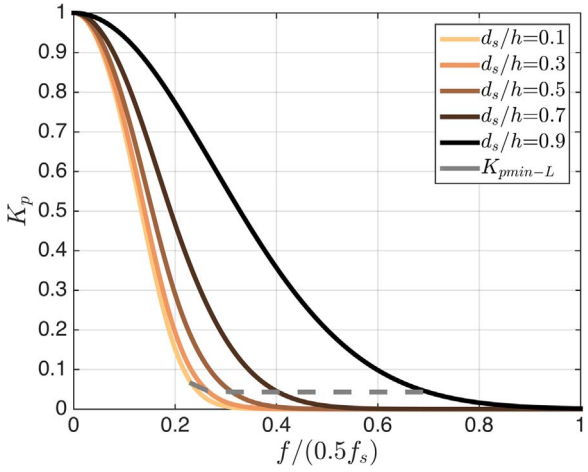

Fig. 1. Schematic trend of K_p versus f for different d_s/h.

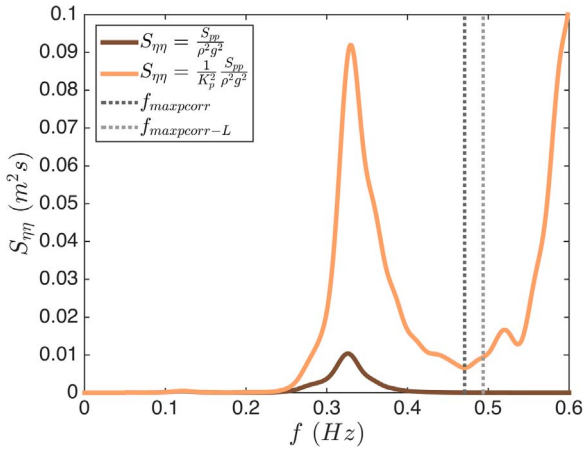

Fig. 2. Effect of K_p on $S_{\eta\eta}$, where $f_{cmin} = 0.05Hz$ and $f_{cmax} = 0.6Hz$.

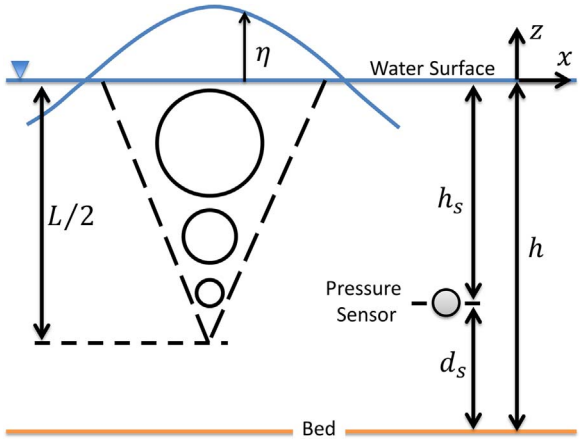

Fig. 3. Schematic sensor deployment setup.

$$f_{maxpcorr-L} = \frac{1}{2\pi}\sqrt{g k_{max-L}\tanh(k_{max-L}h)} = \frac{1}{2\pi}\sqrt{g\frac{\pi}{h-d_s}\tanh\left(\frac{\pi}{h-d_s}h\right)} \tag{7-c}$$

where $\omega = 2\pi f$ is a wave angular frequency. Fig. 4 shows the maximum frequency estimated by the linear wave theory, $f_{maxpcorr-L}$, indicating the frequency beyond which K_p should not be applied. For the case that a pressure sensor sits on a sea bed, i.e. $d_s = 0$, $z = -h = -h_s$ and $k_{max-L}h_s = k_{max-L}h = \pi$, then K_{pmin-L} is:

$$K_{pmin-L}\,(f_{maxpcorr-L}, z = -h) = \frac{\cosh(0)}{\cosh(\pi)} \approx 0.0862 \tag{8-a}$$

$$f_{maxpcorr-L} = \frac{1}{2\pi}\sqrt{g\frac{\pi}{h}\tanh(\pi)} \approx 0.8819 h^{-0.5} \tag{8-b}$$

3.1.5. Practical approach to define lower limit for K_p

Theoretical values derived from the linear wave theory are only applicable to sinusoidal waves. In such conditions, considering $f_{maxpcorr} \approx f_{maxpcorr-L}$ and $K_{pmin} \approx K_{pmin-L}$ leads to acceptable results from the data analysis. However, when a wave profile deviates from a sinusoidal form, as when waves propagate into an intermediate and shallow water depth where their wave forms become skewed, using $f_{maxpcorr-L}$ and K_{pmin-L} for the data analysis are not reasonable anymore. In these conditions, $f_{maxpcorr-L} > f_{maxpcorr}$ and $K_{pmin-L} < K_{pmin}$ (Fig. 5), which leads to an over-estimation of the water surface oscillation and wave energy.

In practice, different approaches are applied in both time and frequency domains to define $f_{maxpcorr}$ and K_{pmin} in order to avoid signal inflation where $f > f_{maxpcorr}$. In the time domain analysis, a maximum value between K_{pmin-L} and a predefined K_{pmin}, i.e. $max\,(K_{pmin-L}, K_{pmin})$, is applied across the board. A constant predefined $K_{pmin} = 0.15$ would be an acceptable choice to avoid amplification of the recorded data greater than 6 times, although this value should be selected based on the waves and water body condition.

In the frequency domain analysis, there are two approaches for defining $f_{maxpcorr}$ and K_{pmin} and preventing signal inflation where $f > f_{maxpcorr}$. In the first approach, a white noise or a noise floor is subtracted from the pressure spectrum before applying K_p into that. In this approach, a uniformly distributed wide band noise for all frequencies is assumed (Bishop and Donelan, 1987; Trowbridge and Elgar, 2001; Smith, 2002; Jones and Monismith, 2007). Subtracting a uniform noise level from a spectrum reflects an assumption that the value of the $f_{maxpcorr}$ is associated with a frequency that a noise floor emerges at the tail of the spectrum (Figs. 6 and 10). In other words, the frequency that a noise floor starts at a tail of the spectrum is associated with the shortest wave that a pressure transducer can detect, and the effects of the shorter waves with larger wave frequencies diminish before reaching the sensor depth. Note that, subtracting a non-uniform noise floor from the spectrum can result in an under-estimation of the results (Jones and Monismith, 2007).

In the second approach, which is the most common one, a high-cutoff frequency is selected to filter out a high frequency section of the spectrum associated with a low signal-to-noise ratio (Bishop and Donelan, 1987; Smith, 2002; Jones and Monismith, 2007). In this method, the high-cutoff frequency can be constant, i.e. $f_{maxpcorr} = f_{cmax}$ = Constant for all situations, or it can be adaptively selected for each burst, i.e. $f_{maxpcorr} = f_{cmax}$ = Adaptive. Selecting a constant cutoff frequency as $f_{maxpcorr} = f_{cmax}$ = Constant is not a straight forward procedure and requires that a series of criteria are met (Jones and Monismith, 2007), and can still result in an incorrect wave calculation (e.g. Van Rijn et al., 2000). Note that, an adaptive cutoff frequency, i.e. $f_{maxpcorr} = f_{cmax}$ = Adaptive, for each burst, can lead to dissimilar conditions from burst to burst and is not recommended.

To overcome the issues associated with the previous approaches, we introduce a modified form of the second approach for defining $f_{maxpcorr}$ and K_{pmin}. In the frequency domain analysis, using a constant high-cutoff frequency, i.e. f_{cmax} = Constant, is an acceptable practice in most cases. However, considering a constant value for $f_{maxpcorr}$ is rarely acceptable and can lead to either over or under-estimation of the wave energy. Therefore, we recommend to use a constant value for f_{cmax} along with adaptive values for $f_{maxpcorr}$ and K_{pmin}, which these adaptive ones are defined for each burst individually. In other words, f_{cmax} = Constant for the entire data series and $f_{maxpcorr}$ = Adaptive for each burst.

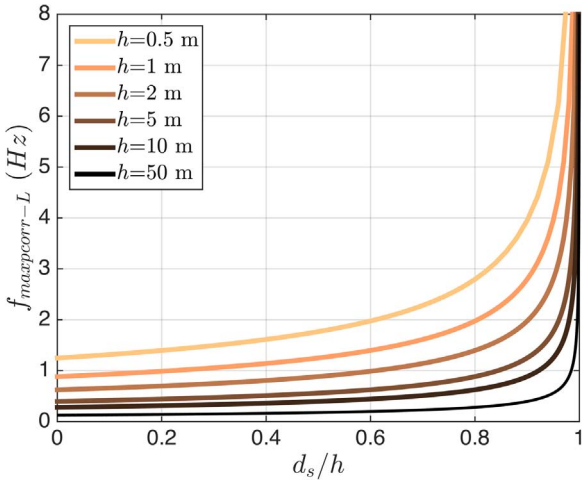

Fig. 4. Maximum frequency estimated by the linear wave theory, $f_{maxpcorr-L}$, beyond which K_p should not be applied.

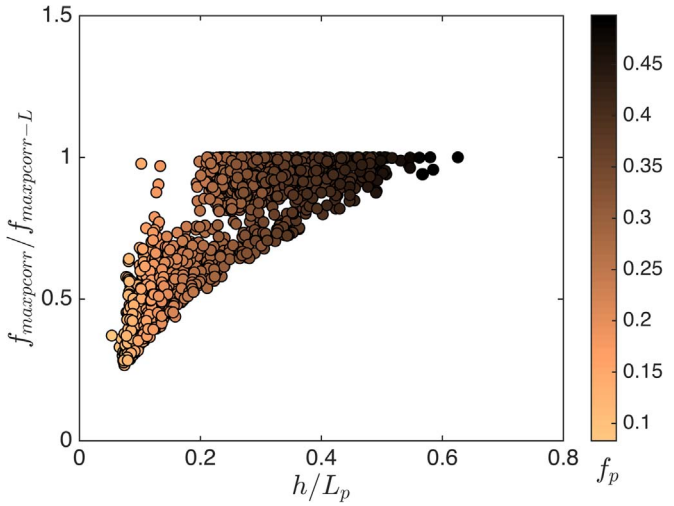

Fig. 5. Relationship between the ratio of $f_{maxpcorr}/f_{maxpcorr-L}$ and relative depth, h/L_p, where L_p is the peak wave length. Color-bar represents f_p. All presented data in this paper are measured in Breton Sound, LA, USA (for detail see Karimpour and Chen, 2016).

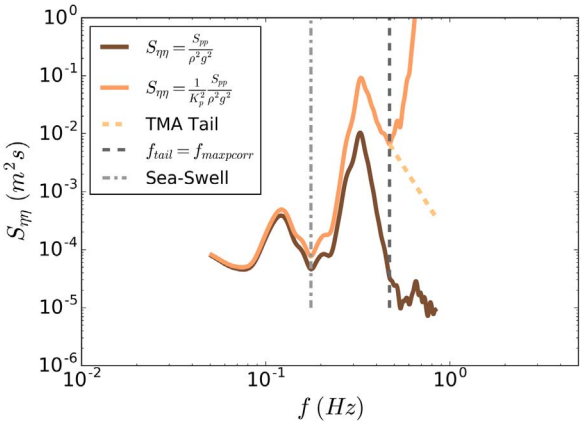

Fig. 6. Replacing a spectrum tail with the TMA spectrum diagnostic tail at $f_{tail}=f_{maxpcorr}=0.47Hz$. The cut-off frequencies are $f_{cmin}=0.05Hz$ and $f_{cmax}=0.835Hz$.

An adaptive value of $f_{maxpcorr}$ can be defined by searching for an exact location of $f_{maxpcorr}$ in the power spectrum. We suggest two methods to find these adaptive $f_{maxpcorr}$ and K_{pmin}. In the first method, adaptive values are found from the power spectral density of the measured water surface elevation before any correction is applied to that, i.e. from $S_{\eta\eta}=S_{PP}/(\rho^2 g^2)$. The $f_{maxpcorr}$ can be located on $S_{\eta\eta}$ by considering that $f_{maxpcorr}$ is the frequency of the shortest wave that the pressure transducer can detect, and typically it is a frequency that a noise floor starts at a tail of the spectrum (Figs. 6 and 10). In the second method, adaptive values are found from a power spectral density of the measured water surface elevation by applying K_p without limiting it to K_{pmin}, i.e. from $S_{\eta\eta}=(1/K_p^2)\times S_{PP}/(\rho^2 g^2)$ where $0\le K_p\le 1$. This causes the tail of the spectrum, after the peak frequency, to drop to a minimum value before it starts to rise toward infinity. The location of this minimum value in the spectrum tail, which is after f_p, is associated with the $f_{maxpcorr}$ (Figs. 6 and 10). After $f_{maxpcorr}$ is defined by either of these methods, the $S_{\eta\eta}$ can be calculated from $S_{\eta\eta}=(1/K_p^2)\times S_{PP}/(\rho^2 g^2)$ where $K_{pmin}\le K_p\le 1$. Note that in this approach, the adaptive $f_{maxpcorr}$ and K_{pmin} should always follow $f_{maxpcorr}\le f_{maxpcorr-L}$ and $K_{pmin}\ge K_{pmin-L}$.

If an adaptive $f_{maxpcorr}$ becomes equal or larger than a constant value chosen for f_{cmax}, then it will be limited to $f_{maxpcorr}=f_{cmax}$, but if an adaptive $f_{maxpcorr}$ is smaller than f_{cmax}, then additional attention is required for applying K_p between $f_{maxpcorr}$ and f_{cmax}. For cases with $f_{maxpcorr}<f_{cmax}$, two approaches can be followed to apply K_p to the data within a frequency range of $f_{maxpcorr}\le f\le f_{cmax}$. In the first approach, the K_p is gradually increased from $K_p=K_{pmin}$ at $f=f_{maxpcorr}-\Delta f_{tr}$ to $K_p=1$ at $f=f_{maxpcorr}+\Delta f_{tr}$ and then it remains 1, i.e. $K_p=1$ for $f_{maxpcorr}+\Delta f_{tr}\le f\le f_{cmax}$. The $\pm\Delta f_{tr}$ defines a frequency range for this transition before and after $f_{maxpcorr}$, and should be selected based on the spectrum's conditions. In the second approach, the K_p values are kept constant as $K_p=K_{pmin}$ for $f_{maxpcorr}\le f\le f_{cmax}$ (Huang and Tsai, 2008). In the second approach, the spectrum tail holds its original slope, while following the first approach leads to a different slope for the spectrum tail compared to the spectrum tail of the measured data.

Note that if there are multiple energy peaks in the spectrum that are associated with higher harmonics of the dominant frequency, particularly with the 2^{nd} harmonic, they should not be mistaken for an amplification effect caused by the application of the small K_p values to the high-frequency section of the spectrum. Therefore, in such cases, an adaptive $f_{maxpcorr}$ should be selected cautiously to reflect the higher harmonic effects without amplifying the noise.

3.2. Wave spectrum diagnostic tail

As was pointed out, a portion of the shorter wave energies within a higher frequency range may completely damp out and diminish in a water column before reaching the pressure sensor depth. In that case, the sensor cannot detect the pressure effect of those high-frequency waves (short waves). Therefore, recorded data within that high frequency range are mostly noise, with an insignificant signal-to-noise ratio. To compensate for the energy that cannot be detected by the sensor, and to prevent an under-estimation of the wave energy from a spectrum, the lost energy of the high-frequency waves needs to be replaced (e.g. Smith et al., 2001; Smith, 2002; Jones and Monismith, 2007). To do that in the frequency domain, at first a simple high-cutoff frequency, f_{tail}, or a low-pass filter, is used to remove a part of the spectrum with a low signal-to-noise ratio. After screening out noise, the lost high-frequency energies are replaced by using an empirical spectrum tail, a so-called diagnostic tail (e.g. Smith, 2002; Jones and Monismith, 2007; Siadatmousavi et al., 2012). For this purpose, the noisy section of the spectrum tail is replaced with the JONSWAP spectrum tail in deep water (Hasselmann et al., 1973), or with the TMA spectrum tail in intermediate and shallow water (Bouws et al., 1985), as illustrated in Figs. 6 and 10. A high-frequency section of the spectrum can be replaced by the JONSWAP diagnostic tail proportional to f^{-n} (Siadatmousavi et al., 2012) as:

$$S_{\eta\eta}(f)=S_{\eta\eta}(f_{tail})\times\left(\frac{f}{f_{tail}}\right)^{-n}\quad \text{for } f>f_{tail} \tag{9}$$

Similarly, the TMA spectrum tail proportional to f^{-n} can be used to replace a high-frequency section of the spectrum as:

$$S_{\eta\eta}(f)=S_{\eta\eta}(f_{tail})\times\frac{\Phi(f,h)}{\Phi(f_{tail},h)}\times\left(\frac{f}{f_{tail}}\right)^{-n}\quad \text{for } f>f_{tail} \tag{10}$$

where f_{tail} is the frequency after which the diagnostic tail is applied, and $S_{\eta\eta}(f_{tail})$ is the value of the spectrum at f_{tail}. In the literature, it is suggested that f_{tail} be set as $f_{tail}=2.5f_m$ (Ardhuin et al., 2010) or $f_{tail}=max(2.5f_m,4f_{mPM})$ (Siadatmousavi et al., 2012), where $f_m=1/T_{m01}$ is the mean wave frequency and f_{mPM} is the mean wave frequency of the Pierson-Moskowitz spectrum (Pierson and Moskowitz, 1964). These recommendations might be too high for the data collected in depth-limited conditions. For these conditions, it is recommended to use $f_p<f_{tail}<1.75f_m$. If data are collected by a pressure sensor, f_{tail} should be set as $f_{tail}=f_{maxpcorr}$, as data with $f_{maxpcorr}<f\le f_{cmax}$ might not be reliable. The n is the tail power coefficient, which defines the tail's slope. The value of n depends on deployment conditions, but typically it is 5 for deep and 3 for shallow water (e.g. Phillips, 1958; Thornton, 1977; Kitaigorodskii, 1983; Miller and Vincent, 1990; Smith, 2002; Jones and Monismith, 2007; Holthuijsen, 2007; Kaihatu et al., 2007;

Siadatmousavi et al., 2012). Then, $n = 4$ might be considered for an intermediate depth. $\Phi = R_{\omega_h}^{-2}(1+(2\omega_h^2 R_{\omega_h})/(\sinh(2\omega_h^2 R_{\omega_h})))^{-1}$ is a transformation function from JONSWAP spectrum in deep water into TMA spectrum in shallow water, where $R_{\omega_h}\tanh(\omega_h^2 R_{\omega_h}) = 1$, and $\omega_h = 2\pi f\sqrt{h/g}$ (Kitaigordskii et al., 1975; Hughes, 1984; Holthuijsen, 2007). The value of Φ can be approximated by $\Phi(f, h)\approx\omega_h^2/2$ for $\omega_h\leq 1$, and $\Phi(f, h)\approx 1 - 0.5(2-\omega_h)^2$ for $1<\omega_h<2$, and $\Phi(f, h) = 1$ for $\omega_h\geq 2$ (Thompson and Vincent, 1983; Bergdahl, 2009).

In general, an implementation of the diagnostic tail for replacement of the measured data is not recommended, unless the high-frequency data are missing due to a low sampling frequency (see Supplementary material A), or due to a deep deployment of the sensor in the water column, or in cases where the high-frequency data are contaminated by noise.

3.3. Sea wave and swell partitioning in a bimodal spectrum

In areas where both wind sea and swell waves are present, the wind sea and swell wave energies can be separated by using a separation frequency, f_{sep}, in a wave power spectrum (e.g., Wang and Gilhousen, 1998; Gilhousen and Hervey, 2001; Portilla et al., 2009; Hwang et al., 2012). The separation frequency, f_{sep}, is a frequency that waves with frequencies $f<f_{sep}$ are swell waves and with $f>f_{sep}$ are wind waves. Methods for separation of the wind sea from swell waves are categorized as an one-dimensional, $1D$, or two-dimensional, $2D$, wind or non-wind based, and can result in a constant or dynamic f_{sep} value. One of the common methods for separation of the wind sea and swell energies is an $1D$ dynamic wind based method, described by Gilhousen and Hervey (2001) as:

$$\xi(f) = \frac{H_{m0}(f)}{L(f)} = \frac{2\pi H_{m0}(f)}{gT_{m02}^2(f)} = \frac{8\pi m_2}{g\sqrt{m_0}} \tag{11-a}$$

$$f_{sep} = max\left(0.75f_x, 0.9\frac{1.25}{U_{10}}\right) \tag{11-b}$$

where $\xi(f)$ is a wave steepness function, L is a wave length, $T_{m02} = \sqrt{m_0/m_2}$ is a mean wave period, $m_n = \int_{f_l}^{f_u} f^n S_{\eta\eta}(f)df$ is the n^{th} moment of the wave spectrum, f_l and $f_u = 0.5Hz$ are the lower and upper limits of the wave spectrum, respectively, and f_x is a frequency associated with a maximum value of $\xi(f)$. The U_{10} is a 10-min average wind velocity observed at 10 m above the surface. A more recent sea-swell partitioning method is described by Hwang et al. (2012) as:

$$I_1(f) = \frac{m_1}{\sqrt{m_{-1}}} \tag{12-a}$$

$$f_{sep} = 24.2084f_{m1}^3 - 9.2021f_{m1}^2 + 1.8906f_{m1} - 0.04286 \tag{12-b}$$

Similarly, $m_n = \int_{f_l}^{f_u} f^n S_{\eta\eta}(f)df$ is the n^{th} moment of the wave spectrum with $f_u = 0.5Hz$, and f_{m1} is a frequency associated with the maximum value of I_1. Figs. 7 and 8 present a separation frequency for sea-swell partitioning, estimated by Gilhousen and Hervey (2001) and Hwang et al. (2012), respectively. Note that, in both of these methods, a f_u larger than $0.5Hz$ might be required for intermediate and shallow water.

3.4. Peak wave frequency from the weighted integral of wave power spectrum

Commonly, peak wave frequency, f_p, and peak wave period, $T_p = 1/f_p$, are obtained directly from the wave power spectrum by locating a frequency associated with a maximum value of $S_{\eta\eta}$. Additionally, peak wave frequency can also be estimated from a weighted integral of the wave power spectrum following Young (1995) as:

$$f_p = \frac{\int (S_{\eta\eta}(f))^5 f df}{\int (S_{\eta\eta}(f))^5 df} \tag{13}$$

Fig. 9 shows that a peak frequency can be accurately estimated from Eq. (13). In general, it is recommended to obtain the f_p directly from a spectrum, unless there are fluctuations in $S_{\eta\eta}$ that prevent an accurate identification of the peak point, in which case Eq. (13) is suggested.

4. Toolbox overview

Ocean Wave Analyzing Toolbox, OCEANLYZ, is a MATLAB toolbox developed for analyzing wave data time series collected in a laboratory or in water bodies such as oceans, seas, and lakes. This toolbox contains a number of MATLAB functions aimed at wave analysis in the time and frequency domains by using the zero-crossing and spectral analysis methods, respectively. It can output the wave properties such as a zero-moment wave height, H_{m0}, significant wave height, H_s, mean wave height, H_z, peak wave period, T_p, and mean period, T_z. This toolbox has been under development since 2012, as a part of the field data collection and analysis program in the depth-limited estuaries of Louisiana, USA. OCEANLYZ has evolved over time to address the issues which have arisen associated with the shallow water data analysis.

This toolbox can apply the pressure response factor, K_p, in both time and frequency domains to account for pressure attenuation and energy loss when the data are collected by a pressure sensor. The $f_{maxpcorr}$ value, which is a maximum frequency to apply K_p, can be either predefined by a user or can be calculated adaptively within the code. The toolbox can replace the high-frequency section of the spectrum with either the JONSWAP or TMA diagnostic tail. If swell is present, the wind sea and swell energies can be partitioned and reported by using the Hwang et al. (2012) method. In this toolbox, a peak wave period is obtained directly from a power spectrum peak, while a peak wave frequency is calculated from a weighted integral of the wave power spectrum, i.e. Eq. (13). Water surface elevation power spectral density along with the required inputs for spectral analysis in OCEANLYZ are schematically illustrated in a logarithmic scale in Fig. 10.

To evaluate the toolbox's outcomes, in addition to extensive tests with field data, OCEANLYZ's performance was tested with a series of numerically generated linear and random waves. For this purpose, at first, a time series of the linear waves was used to assess its performance. Next, a time series of random waves based on the JONSWAP spectrum was generated and used as a test case to assess

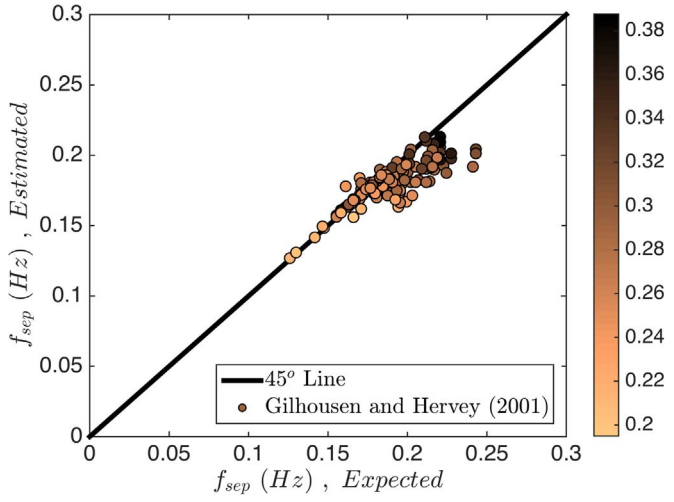

Fig. 7. Evaluating swell and wind sea energy separation using the Gilhousen and Hervey (2001) method. Color-bar represents h/L_p.

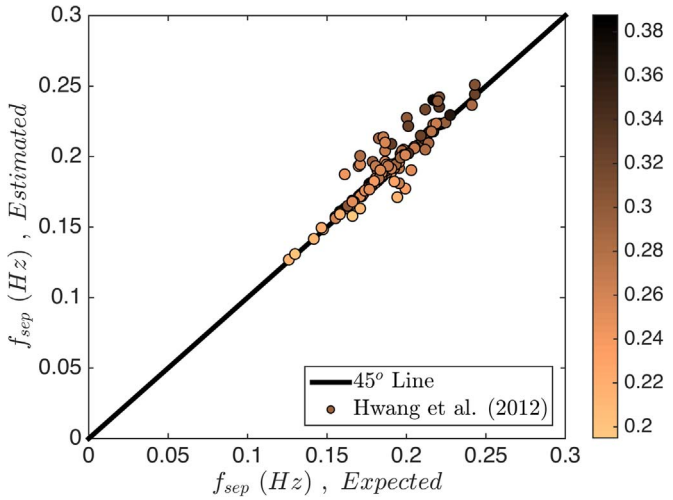

Fig. 8. Evaluating swell and wind sea energy separation using the Hwang et al. (2012) method. Color-bar represents h/L_p.

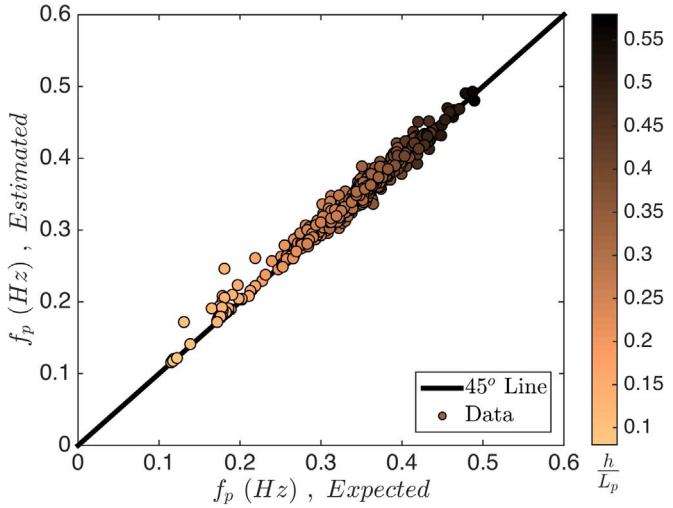

Fig. 9. Evaluating a peak wave frequency estimation from a weighted integral of the wave power spectrum. Color-bar represents h/L_p.

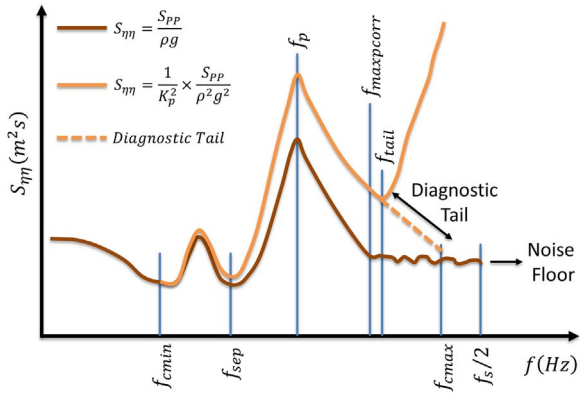

Fig. 10. Schematic log-log scale plot of $S_{\eta\eta}$ versus f. Here, $f_{maxpcorr} < f_{tail}$ but it can be set as $f_{maxpcorr} = f_{tail}$.

the accuracy of the wave properties estimation. The root-mean-square error for N paired samples of (X, Y), where X and Y are the expected and estimated values, respectively, can be calculated from $RMSE = \sqrt{\sum (Y_i - X_i)^2/N}$. The $RMSE$ value for 1000 sets of data was $0.0099m$ for H_{m0} and was $6.0585 \times 10^{-4} Hz$ for $f_p = 1/T_p$. The coefficient

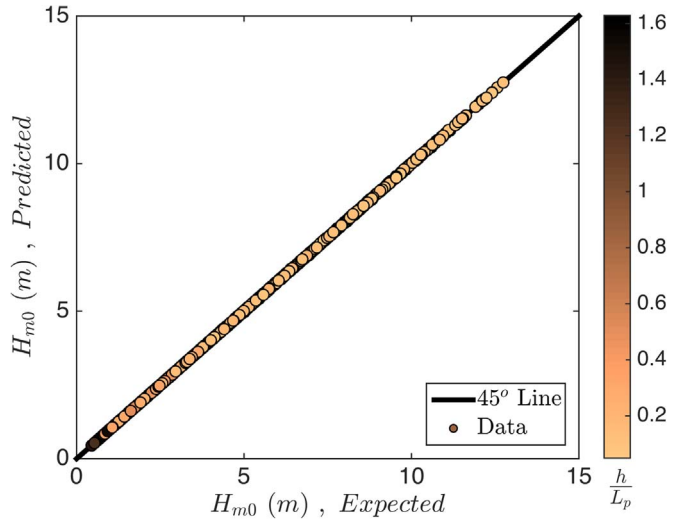

Fig. 11. Evaluating the accuracy of OCEANLYZ in the estimation of H_{m0}. Color-bar represents h/L_p.

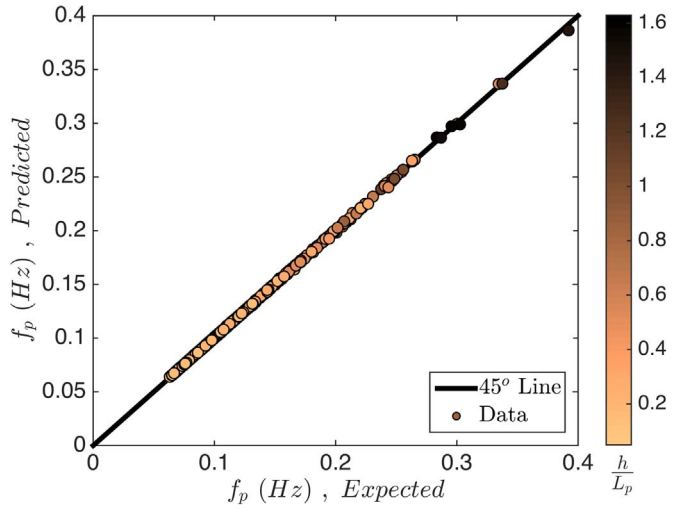

Fig. 12. Evaluating the accuracy of OCEANLYZ in the estimation of f_p. Color-bar represents h/L_p.

of determination, R^2, between the expected and estimated values was 0.99 for both H_{m0} and $f_p = 1/T_p$. Figs. 11 and 12 illustrate the expected values versus those calculated by the OCEANLYZ.

5. Conclusions

There are a number of well established methods in the literature for an accurate analysis of measured wave data and a precise estimation of the wave parameters. However, obtaining reliable results requires knowledge of the behavior, strengths and weaknesses of those methods, otherwise the quality of the results might be questionable. More importantly, an implementation of those methods in depth-limited water bodies, like estuaries and lakes, requires additional attention in order to acquire correct wave parameters.

This paper describes potential issues associated with the analysis of pressure transducer data and provides possible solutions. Wave measurement and analysis particularly in depth-limited water bodies are discussed and potential issues for obtaining reliable results in these environments are explained. The procedure for converting pressure data into water surface elevation data, treating the high frequency data with a low signal-to-noise ratio, partitioning swell and wind sea energies, and estimating the peak wave frequency from a weighted

integral of the wave power spectrum are described. Detailed explanations are provided on how to convert pressure data acquired with a pressure transducer into water surface elevation and on how to recover energy losses associated with pressure attenuation in depth. Potential sources of errors during data analysis are discussed. It is shown how an improper implementation of these methods can lead to incorrect outcomes, and it is explained how to minimize errors associated with the influential parameters.

Furthermore, to provide researchers with a tool for a reliable estimation of the wave parameters, particularly in shallow and intermediate water, the Ocean Wave Analyzing toolbox, OCEANLYZ, is introduced. The toolbox contains a number of MATLAB functions for estimation of the wave properties in the time and frequency domains. The toolbox has been developed and examined during a number of field studies in Louisiana estuaries.

Acknowledgments

The study was supported in part by the National Science Foundation (NSF Grant SEES-1427389, and CCF-1539567) and the Louisiana Sea Grant. Ranjit Jadhav and the CSI field support group at the Louisiana State University assisted in the field experiments. Comments from Cody Johnson improved the manuscript. Any opinions, findings, conclusions and recommendations expressed in this paper are those of the authors and do not necessarily reflect the views of the NSF or NOAA. Fig. 6 in this publication was produced by Matplotlib (Hunter, 2007).

Appendix A. Supplementary material

Supplementary data associated with this article can be found in the online version at doi:10.1016/j.cageo.2017.06.010.

References

Ardhuin, F., Rogers, E., Babanin, A.V., Filipot, J.F., Magne, R., Roland, A., Collard, F., 2010. Semiempirical dissipation source functions for ocean waves. Part I: definition, calibration, and validation. J. Phys. Oceanogr. 40 (9), 1917–1941.

Beji, S., 2013. Improved explicit approximation of linear dispersion relationship for gravity waves. Coast. Eng. 73, 11–12.

Bergdahl, L., 2009. Comparison of measured shallow-water wave spectra with theoretical spectra. In Proceedings of the 8th European Wave and Tidal Energy conference pp. 100–105.

Bishop, C.T., Donelan, M.A., 1987. Measuring waves with pressure transducers. Coast. Eng. 11 (4), 309–328.

Bouws, E., Günther, H., Rosenthal, W., Vincent, C.L., 1985. Similarity of the wind wave spectrum in finite depth water: 1. spectral form. J. Geophys. Res.: Oceans 90 (C1), 975–986.

Cavaleri, L., 1980. Wave measurement using pressure transducer. Oceanol. Acta 3 (3), 339–346.

Chakrabarti, S.K., 1987. Hydrodynamics of Offshore Structures. WIT press.

Dean, R.G., Dalrymple, R.A., 1991. Water wave mechanics for engineers and scientists.

Gilhousen, D.B., Hervey, R., 2001. Improved Estimates of Swell from Moored Buoys (Proceedings of the Fourth International Symposium WAVES 2001). ASCE, Alexandria, VA, 387–393.

Hashimoto, N., Thurston, S.W., Mitsui, M, 1997. Surface wave recovery from subsurface pressure records on the basis of weakly nonlinear directional wave theory. In: Hemsley, B.L.E.A.M. [ed.], Ocean wave measurement and analysis. Proceedings of the Third International Symposium Waves 97 held in Virginia Beach, Virginia, November 3–7, 1997, American Society of Civil Engineers Publications, p. 869-882.

Hasselmann, K., Barnett, T.P., Bouws, E., Carlson, H., Cartwright, D.E., Enke, K., Ewing, J.A., Gienapp, H., Hasselmann, D.E., Kruseman, P., Meerbrug, A., Muller, P., Olbers, D.J., Richter, K., Sell, W., Walden, H., 1973. Measurements of wind-wave growth and swell decay during the joint North Sea Wave Project (JONSWAP). Dtsch. Hydrogr. Z. A80 (12), (95p).

Holthuijsen, L.H., 2007. Waves in Oceanic and Coastal Waters. Cambridge University Press.

Huang, M.C., Tsai, C.H., 2008. Pressure transfer function in time and time-frequency domains. Ocean Eng. 35 (11), 1203–1210.

Hughes, S.A., 1984. The TMA shallow-water spectrum description and applications (No. CERC-TR-84-7). Coastal Engineering Research Center Vicksburg MS.

Hunt, J.N., 1979. Direct solution of wave dispersion equation. J. Waterw. Port. Coast. Ocean Div. 105 (4), 457–459.

Hunter, J.D., 2007. Matplotlib: a 2D graphics environment. Comput. Sci. Eng. 9 (3), 90–95.

Hwang, P.A., Ocampo-Torres, F.J., García-Nava, H., 2012. Wind sea and swell separation of 1D wave spectrum by a spectrum integration method. J. Atmos. Ocean. Technol. 29 (1), 116–128.

Jones, N.L., Monismith, S.G., 2007. Measuring short-period wind waves in a tidally forced environment with a subsurface pressure gauge. Limnol. Oceanogr.: Methods 5 (10), 317–327.

Kaihatu, J.M., Veeramony, J., Edwards, K.L., Kirby, J.T., 2007. Asymptotic behaviour of frequency and wave number spectra of nearshore shoaling and breaking waves. J. Geophys. Res. 112, C06016.

Karimpour, A., Chen, Q., 2016. A simplified parametric model for fetch-limited peak wave frequency in shallow estuaries. J. Coast. Res. 32 (4), 954–965.

Karimpour, A., Chen, Q., Twilley, R.R., 2016. A field study of how wind waves and currents may contribute to the deterioration of saltmarsh fringe. Estuaries Coasts, 39–935.

Karimpour, A., Chen, Q., Twilley, R.R., 2017. Wind wave behavior in fetch and depth limited estuaries. Sci. Rep. 7, 40654.

Kitaigordskii, S.A., Krasitskii, V.P., Zaslavskii, M.M., 1975. On Phillips' theory of equilibrium range in the spectra of wind-generated gravity waves. J. Phys. Oceanogr. 5 (3), 410–420.

Kitaigorodskii, S.A., 1983. On the theory of the equilibrium range in the spectrum of wind-generated gravity waves. J. Phys. Oceanogr. 13 (5), 816–827.

Kuo, Y.Y., Chiu, Y.F., 1994. Transfer function between wave height and wave pressure for progressive waves. Coast. Eng. 23 (1), 81–93.

Landry, B.J., Hancock, M.J., Mei, C.C., García, M.H., 2012. WaveAR: a software tool for calculating parameters for water waves with incident and reflected components. Comput. Geosci. 46, 38–43.

Lee, D.Y., Wang, H., 1984. Measurement of surface waves from subsurface gage. Coastal Engineering Proceedings, 1(19).

McCormick, M.E., 2009. Ocean Engineering Mechanics: With Applications. Cambridge University Press.

Miller, H.C., Vincent, C.L., 1990. FRF spectrum: TMA with Kitaigorodskii's f-4 scaling. J. Waterw. Port Coast. Ocean Eng. 116 (1), 57–78.

Phillips, O.M., 1958. The equilibrium range in the spectrum of wind-generated waves. J. Fluid Mech. 4 (04), 426–434.

Pierson, W.J., Moskowitz, L., 1964. A proposed spectral form for fully developed wind seas based on the similarity theory of SA Kitaigorodskii. J. Geophys. Res. 69 (24), 5181–5190.

Portilla, J., Ocampo-Torres, F.J., Monbaliu, J., 2009. Spectral partitioning and identification of wind sea and swell. J. Atmos. Ocean Technol. 26, 107–122.

Reeve, D., Chadwick, A., Fleming, C., 2012. Coastal Engineering: Process, Theory, and Design Practice 2nd ed.. Spon, New York.

Siadatmousavi, S.M., Jose, F., Stone, G.W., 2012. On the Importance of High Frequency Tail in Third Generation Wave Models. Coastal Engineering.

Smith, J.M., 2002. Wave pressure gauge analysis with current. J. Waterw., Port Coast. Ocean Eng. 128 (6), 271–275.

Smith, M.J., Stevens, C.L., Gorman, R.M., McGregor, J.A., Neilson, C.G., 2001. Wind-wave development across a large shallow intertidal estuary: a case study of Manukau Harbour, New Zealand. N.Z. J. Mar. Freshw. Res. 35 (5), 985–1000.

Thompson, E.F., Vincent, C.L., 1983. Prediction of Wave Height in Shallow Water (Proceedings of Coastal Structures 1983). American Society of Civil Engineers, 1000–1008.

Thornton, E.B., 1977. Rederivation of the saturation range in the frequency spectrum of wind-generated gravity waves. J. Phys. Oceanogr. 7 (1), 137–140.

Townsend, M., Fenton, J.D., 1996. A comparison of analysis methods for wave pressure data. Coastal Engineering Proceedings, 1(25).

Trowbridge, J., Elgar, S., 2001. Turbulence measurements in the surf zone*. J. Phys. Oceanogr. 31 (8), 2403–2417.

Tsai, C.H., Young, F.J., Lin, Y.C., Li, H.W., 2001. Comparison of methods for recovering surface waves from pressure transducers. In Ocean Wave Measurement and Analysis In: Proceedings of the 4th International Symposium, WAVES pp. 347–356.

Tsai, C.H., Huang, M.C., Young, F.J., Lin, Y.C., Li, H.W., 2005. On the recovery of surface wave by pressure transfer function. Ocean Eng. 32 (10), 1247–1259.

Van Rijn, L.C., Grasmeijer, B.T., Ruessink, B.G., 2000. Measurement errors of instruments for velocity, wave height, sand concentration and bed levels in field conditions. Deltares (WL)-Utrecht University.

Wang, D., Gilhousen, D., 1998. Separation of seas and swells from NDBC buoy wave data (Fifth Int. Workshop on Wave Hindcasting and Forecasting). ASCE, Melbourne, FL, 155–162.

Wang, H., Lee, D.Y., Garcia, A., 1986. Time series surface-wave recovery from pressure gage. Coast. Eng. 10 (4), 379–393.

Young, I.R., 1995. The determination of confidence limits associated with estimates of the spectral peak frequency. Ocean Eng. 22, 669–686.